Fluorescence of *all-trans*-Retinal as a Crystal and in a Dense Solution Phase

Laura Moroni, Cristina Gellini, Pier Remigio Salvi,* and Vincenzo Schettino

Laboratorio di Spettroscopia Molecolare, Dipartimento di Chimica, Via Gino Capponi 9, 50121 Firenze, Italy

Received: June 12, 2000; In Final Form: September 19, 2000

The fluorescence spectra of *all-trans*-retinal as a polycrystalline solid and in highly concentrated *n*-hexane solutions have been measured at 77 K as a function of the exciting wavelength between 420 and 500 nm, i.e., below the energy of the lowest excited state of *all-trans*-retinal. The fluorescence spectra of concentrated solutions have been deconvolved in terms of four Gaussian bands, independent of the excitation wavelength. Emissions from complexes with water and from retinal dimers have been assigned in the solution spectrum, in agreement with early reports. Stable 1:1 and 1:2 complexes with protic solvents (H_2O, CH_3OH, C_2H_5OH, phenol) have been calculated by ab initio density functional (DF) methods (B3-LYP/6-31G*), enforcing the experimental assignment. Due to extensive drying operations on the solid, the fluorescence from water complexes is negligible in the crystal spectrum of *all-trans*-retinal. In this case the fluorescence has been attributed to dimers and higher order clusters. DF calculations on the isolated dimer and tetramer as well as on the same species of a retinal homologue indicate that these systems are stable. Dimers and tetramers of *all-trans*-retinal may be identified in the crystal structure, justifying the fluorescence from these species in the crystal spectrum.

I. Introduction

Photophysical and photochemical properties of retinal chromophores, and in particular of *all-trans*-retinal, have been for a long time the object of considerable interest due to their biochemical role in photoactive proteins such as rhodopsin and bacteriorhodopsin.[1−5] The fluorescence and photoisomerization quantum yields of *all-trans*-retinal in solution depend on the solvent medium, increasing from aprotic nonpolar solvents to protic solvents because of hydrogen bond formation.[6−9] Correspondingly, the yield of intersystem crossing decreases.[10−13] The solvent dependence has been related to the change of excited-state ordering in hydrogen-bonded retinal.[6,8] While it is well-established on experimental[14−17] and theoretical grounds[14,18−21] that the strongly absorbing B_u-like $\pi\pi^*$ state ("B_u^+", according to the approximate symmetry classification by quotation marks derived by correlation with $\pi\pi^*$ states of linear C_{2h} polyenes)[18] is at energy higher than the doubly excited A_g-like $\pi\pi^*$ state ("A_g^-"), it has been generally assumed[8,22,23] that in aprotic nonpolar solvents the lowest excited, S_1, state is $n\pi^*$ and the second, S_2, is "A_g^-" and that the order is reversed in protic solvents.

Femtosecond time-resolved experiments have recently given conclusive indications on the ultrafast relaxation of *all-trans*-retinal from the singlet manifold in aprotic and protic solvents and further information on the state ordering.[13,24−26] The molecular fluorescence in *n*-hexane at room temperature consists of three components: one extremely fast ($\tau = 30$ fs, $\lambda_{max} \approx 430$ nm), a second fast ($\tau = 370$ fs, $\lambda_{max} \approx 440$ nm), and the third slow ($\tau = 33.5$ ps, $\lambda_{max} \approx 560$ nm), which have been assigned as emissions from S_3("B_u^+"), S_2("A_g^-"), and $S_1(n\pi^*)$, respectively.[24] Second, the study of the formation and dissociation of the hydrogen-bonded complex with 1-butanol in the mixed cyclohexane/1-butanol solvent by femtosecond transient absorption indicates that (i) no change in the state ordering between the $n\pi^*$ and "A_g^-" states occurs upon hydrogen bond formation and (ii) hydrogen-bonded retinal may fluoresce from S_2("A_g^-") rather than from $S_1(n\pi^*)$.[26]

In addition to molecular and complex fluorescence, a third type of fluorescence, due to retinal dimers, was earlier reported and found to be responsible for the emission from retinal solutions at high concentration.[27] The result is important for understanding the relaxation dynamics of crystalline *all-trans*-retinal. In the course of a Raman study on low-frequency vibrations of *all-trans*-retinal, we have preliminarly reported on an unexpected broad crystal emission obscuring Raman peaks, observed at low temperature with an excitation energy below that of the S_1 state.[28] This prompted us to study in more detail how the emission properties change from solution to crystal. In this paper we report on the fluorescence of *all-trans*-retinal (ATR; see Figure 1) in highly concentrated *n*-hexane solutions and as a solid at low temperature. Combining crystal and solution results with accurate density functional (DF) calculations on retinal clusters and protic complexes, the fluorescence with maximum around 18220 cm^{-1} (≈549 nm) is assigned to dimers of ATR. A second emission band, occurring at 16900 cm^{-1} (≈591 nm) and with an excitation counterpart at 20800 cm^{-1}(≈480 nm), is assigned to tetramers.

II. Experimental Section

ATR was received from Sigma-Aldrich in sealed ampules at dry ice temperature. The sample purity was checked by thin-layer chromatography according to a reported procedure.[7] The material was transferred in a glass bulb connected to a vacuum line, dried under dynamic vacuum for ≈24 h, and conserved under vacuum in the dark at −20 °C. Before each experiment, the polycrystalline sample was inserted in a small quartz cell, 0.2 cm thick, placed in a drybox under dry nitrogen flow to avoid wetting, quickly disaerated with several thaw−freeze pumping cycles, and then degassed to high vacuum ($\leq 10^{-4}$

* To whom correspondence should be addressed. E-mail: salvi@chim.unifi.it.

10.1021/jp002098+ CCC: $19.00
Published on Web 11/01/2000

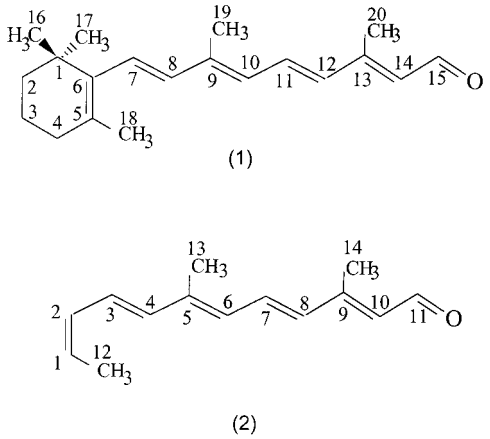

(1)

(2)

Figure 1. Molecular structure of *all-trans* retinal **1** (ATR) and its homologue 2-*s*-*cis*,4-*s*-*trans*,6-*s*-*trans*,8-*s*-*trans*,10-*s*-*trans*,1,5,9-trimethyldecapentanal (**2**, HATR) with atomic numbering.

Torr) for 1 day. This procedure was also followed for the preparation of solutions of ATR in spectroscopic grade *n*-hexane. Low-temperature measurements were performed with a homemade cryostat plunging directly into liquid nitrogen the quartz cell with the polycrystalline or the solution sample.

The experimental setup for fluorescence measurements has been described in previous reports.[29,30] Only some points of interest for the present experiments will be reported here. ATR is excited by the third harmonic of a Nd:YAG pulsed laser operating at 10 Hz or by a tunable OPO laser (420−550 nm tuning range). Excitation bandwidths of ≈1 and ≈20 cm^{-1} in the two cases and emission band-pass of ≈50 cm^{-1} were used in fluorescence experiments. Second, the exciting beam was mildly focused on the crystal to avoid sample heating. The pulse energy was ≈10^{-2} mJ on the sample, independent of the excitation wavelength. Third, all the fluorescence spectra were normalized to a reference signal taken by diverting a small portion of the incident intensity on a photodiode.

Fluorescence spectra have been also measured at 77 K on ATR solutions in 3-methylpentane (3-MeP), *n*-hexane, and ethanol (all solvents spectroscopic grade) with a JASCO FP 750 instrument (emission and excitation band-passes, 10 nm). The results were found in complete agreement with those of past reports.[6−8] Fluorescence spectra of the same solutions were taken exciting with our laser system. In this case the excitation and emission bandwidths are much smaller than the inhomogeneous width of the first absorption band of ATR.[31] The 3-MeP and ethanol solutions prepared at 77 K show good optical transparency in the concentration range 10^{-4}−10^{-5} M.

Standard absorption spectra at room and low temperature have been measured with a Cary 14 spectrophotometer.

III. Results

The fluorescence spectra of ATR 10^{-2} M in *n*-hexane and as a polycrystalline sample, measured at 77 K with excitation wavelength varying between 420 and 500 nm (≈24000−20000 cm^{-1}), are shown in Figures 2 and 3, respectively. In both cases a broad emission extending up to ≈15000 cm^{-1} and with maximum slightly red-shifted with decreasing excitation wavenumber is found. Fluorescence is observed even exciting the solution and the solid at 500 nm, i.e., with photon energies well below that of the lowest excited state in the molecule and in the crystal. In fact, for the molecule in aprotic nonpolar solvents spectroscopic[23,32] and time-resolved[24] studies indicate that the $n\pi^*$ and "A_g^-" levels are close in energy with $n\pi^*$ being at

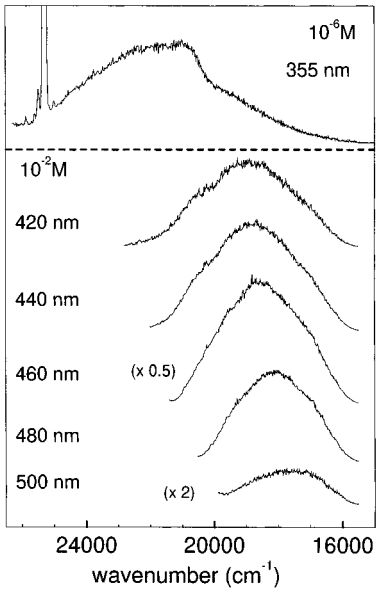

Figure 2. Bottom: Fluorescence spectra of ATR in *n*-hexane solution, $c = 10^{-2}$ M, at 77 K as a function of the excitation wavelength in the range 420−500 nm. Top: fluorescence spectrum of ATR in *n*-hexane solution, $c = 10^{-6}$ M, at 77 K with $\lambda_{exc} = 355$ nm. The energy of the excitation pulse is 10^{-2} mJ on the sample, independent of the excitation wavelength.

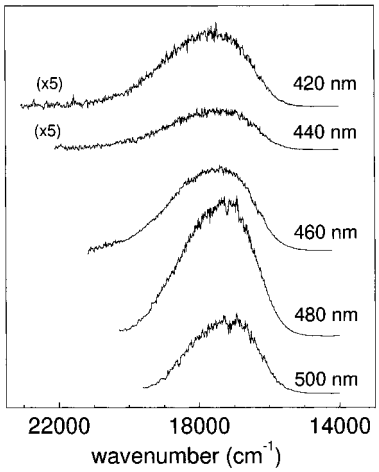

Figure 3. Fluorescence spectra of polycrystalline ATR at 77 K as a function of the excitation wavelength in the range 420−500 nm. The energy of the excitation pulse is 10^{-2} mJ on the sample, independent of the excitation wavelength.

lower energy,[24] and located between 24000 and 23000 cm^{-1} (≈416−434 nm). As to the crystal, the one-photon absorption spectrum consists of a strong $S_0 \rightarrow$ "B_u^+" band with maximum at 25800 cm^{-1} (≈387 nm) and a low-lying shoulder at 23900 cm^{-1} (≈418 nm), assigned to the $S_0 \rightarrow$ "A_g^-" transition.[15,16] Although the $S_0 \rightarrow n\pi^*$ crystal transition has not yet been observed, the substantial similarity of the crystal spectrum[16,33] with one-photon solution data[34−36] suggests the occurrence of the $n\pi^*$ level in the same energy range of the $S_0 \rightarrow$ "A_g^-" transition.

Let us first discuss the solution data. Evidence of dimer formation in solution with increasing retinal concentration has been already reported, and a partial sandwich structure with overlapping polyenic chains, of the type ⇄, has been proposed for the dimer.[27] As no structural data are available, DF calculations were performed for geometrical optimization using the 6-31G* basis set and the B3-LYP exchange correlation

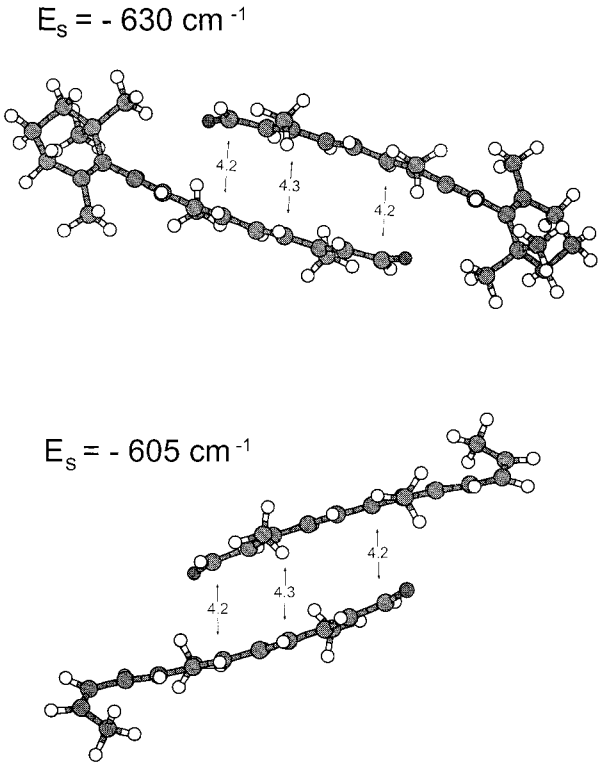

Figure 4. Calculated structure (side view) of $(ATR)_2$ and $(HATR)_2$ (DF calculation, B3-LYP functional, 6-31G* basis set) with relevant intermolecular distances (Å). The two polyenic chains overlap with C_9 of one monomer above O of the other and vice versa. The average intrapair distances are 4.25 and 4.23 Å for $(ATR)_2$ and $(HATR)_2$, respectively. For each dimer the stabilization energy (E_s, cm^{-1}) is indicated on the upper left.

functional.[37,38] This type of calculation was already applied with success to the vibrational analysis of low-frequency ATR modes.[28] The result is shown in Figure 4. The two polyenic units overlap, with C_9 of one monomer above O of the other and vice versa, at an average distance of 4.25 Å and bend slightly with respect to each other at the C═O end. The dimer is more stable than the component units by 630 cm^{-1} (E_s = -630 cm^{-1}), taking into account the basis set superposition error (BSSE).[39,40] For the sake of comparison similar calculations have been performed on the retinal homologue **2** (2-*s*-*cis*,4-*s*-*trans*,6-*s*-*trans*,8-*s*-*trans*,10-*s*-*trans*,1,5,9-trimethyldecapentanal, HATR; see Figure 1) as its polyenic unit mimics the retinal chain. $(HATR)_2$ has geometry and stability similar to those of $(ATR)_2$ (see Figure 4), suggesting that $\pi\pi^*$ interactions are mostly responsible of the dimer stability in both cases.

The fluorescence spectra of the solution, in particular with $\lambda_{exc} = 420$, 440 nm, show a weak band at ≈21000 cm^{-1} related, in agreement with past assignments,[6−8] to hydrogen-bonded complexes. To check this point, the fluorescence emission of ATR (10^{-5} M) in *n*-hexane and ethanol at 77 K upon broad- and narrow-band excitation ($\lambda_{exc} = 355$ nm) has been measured (see Figure 5). As reported,[6−8] a single fluorescence band is observed in the first case. On the contrary, the narrow-band excited spectrum shows a structure in the same emission region with a band, more prominent in the protic solvent, and a shoulder having maxima around 21000 and 19500 cm^{-1}, respectively. This may be justified noting that laser-excited fluorescence from matrixes is related to the selective excitation of a portion of molecules among all those contributing to the inhomogeneous absorption profile, giving rise to better resolved spectra than with broad excitation.[41] In the case of ATR the inhomogeneous

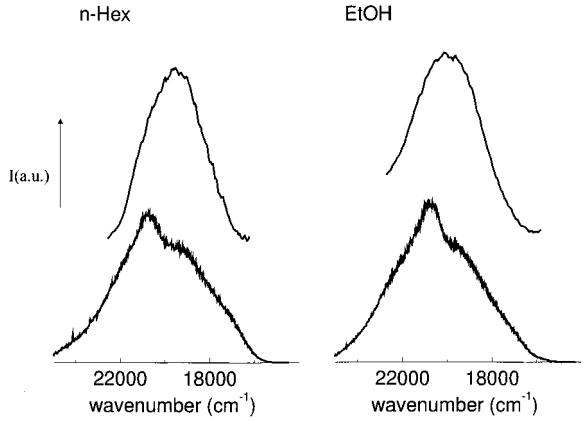

Figure 5. Narrow-band (bottom) and conventional (top) fluorescence spectra of ATR in *n*-hexane and ethanol (*n*-Hex and EtOH, respectively, $c = 10^{-5}$ M) at 77 K. Bottom: $\lambda_{exc} = 355$ nm; $\Delta\omega_{exc} \approx 1$ cm^{-1}; $\Delta\omega_{em} \approx 50$ cm^{-1}. Top: $\lambda_{exc} = 355$ nm; $\Delta\lambda_{exc} = \Delta\lambda_{em} = 10$ nm.

broadening of the first absorption band has been discussed in detail in several papers.[31,35,42] In principle, the low-energy shoulder may be interpreted either as a vibronic addition to the 21000 cm^{-1} band or as emission from a second fluorescent system. However, in favor of the latter choice there is the fact that the relative intensity of the two bands is not constant but rather depends strongly on the solute concentration. On the other hand, DF calculations show that not only 1:1 but also 1:2 complexes of ATR with protic donors such as water, methanol, ethanol, and phenol are stable. The relevant parameters of the optimized geometries (DF/B3-LYP calculations, 6-31G* basis set) and the stabilization energies, including the BSSE correction, are collected in Table 1. Short O···H distances are predicted for all 1:1 complexes, the smallest (1.794 Å) being relative to that with phenol. Correspondingly, this latter has the largest stability ($E_s = -3220$ cm^{-1}) among the four considered. The 1:2 complexes are formed with energies roughly twice those of the 1:1 complexes and O···H distances slightly increased with respect to the 1:1 geometries, except for ethanol. In this case the 1:2 complex has, apparently due to steric hindrance, two quite different O···H distances, both longer than O···H of the 1:1 complex. A detailed view of the 1:1 and 1:2 complexes of ATR with water and ethanol is provided in Figure 6. The protic molecules are bound to ATR through the C═O end, and in particular for the 1:2 complexes, both ligands are directed toward the carbonylic group. Thus, an assignment of the structured emission profile to the $S_2(\text{“}A_g^-\text{”}) \rightarrow S_0$ fluorescence of the 1:1 and 1:2 complexes is plausible, with the 1:2 component shifted to lower energy with respect to the 1:1 complex of an amount comparable to that from the free molecule (band maximum at ≈22400 cm^{-1})[24] to the 1:1 complex.

With these considerations in mind it has been assumed that the solution spectrum results from the combination of the $S_2(\text{“}A_g^-\text{”}) \rightarrow S_0$ fluorescence bands of the 1:1 and 1:2 protic complexes and that of the retinal dimer. A deconvolution procedure has been adopted in order to specify the basic contributions as a function of the exciting wavelength. For best fit to experimental data a fourth component band has been added in the low-energy region of the fluorescence spectrum. Good agreement with observed spectra is reached with center frequencies and widths of the component bands, assumed Gaussian, independent of λ_{exc}, as intuitively expected, and taking as the only adjustable parameter the band maxima. The fitted parameters are reported in Table 2, and a typical result is shown in Figure 7, bottom panel. From the deconvolution data it follows that the dimer emission band, denoted as D in Table 2 and

TABLE 1: 1:1 and 1:2 Complexes of ATR with Water, Methanol (MeOH), Ethanol (EtOH), and Phenol (PhOH) According to DF Calculations Using the 6-31G* Basis Set and the B3-LYP Exchange Correlation Functional[a]

	O···H (Å)	E_s (cm^{-1})		O···H (Å)	E_s (cm^{-1})
ATR···H_2O	1.909	−1980	ATR···EtOH	1.881	−2036
ATR···$(H_2O)_2$	1.928	−3980	ATR···$(EtOH)_2$	1.951	−3040
	1.938			2.105	
ATR···MeOH	1.877	−2060	ATR···PhOH	1.794	−3220
ATR···$(MeOH)_2$	1.906	−3970	ATR···$(PhOH)_2$	1.833	−6030
	1.912			1.846	

[a] O···H, hydrogen bond distance; E_s, stabilization energy with respect to components, taking into account the BSSE correction (see text for details). C=C and C=O bond lengths of the polyenic chain in ATR are respectively C_7=C_8 = 1.354 Å, C_9=C_{10} = 1.368 Å, C_{11}=C_{12} = 1.361 Å, C_{13}=C_{14} = 1.366 Å, C_{15}=O = 1.223 Å and do not change appreciably in all complexes.

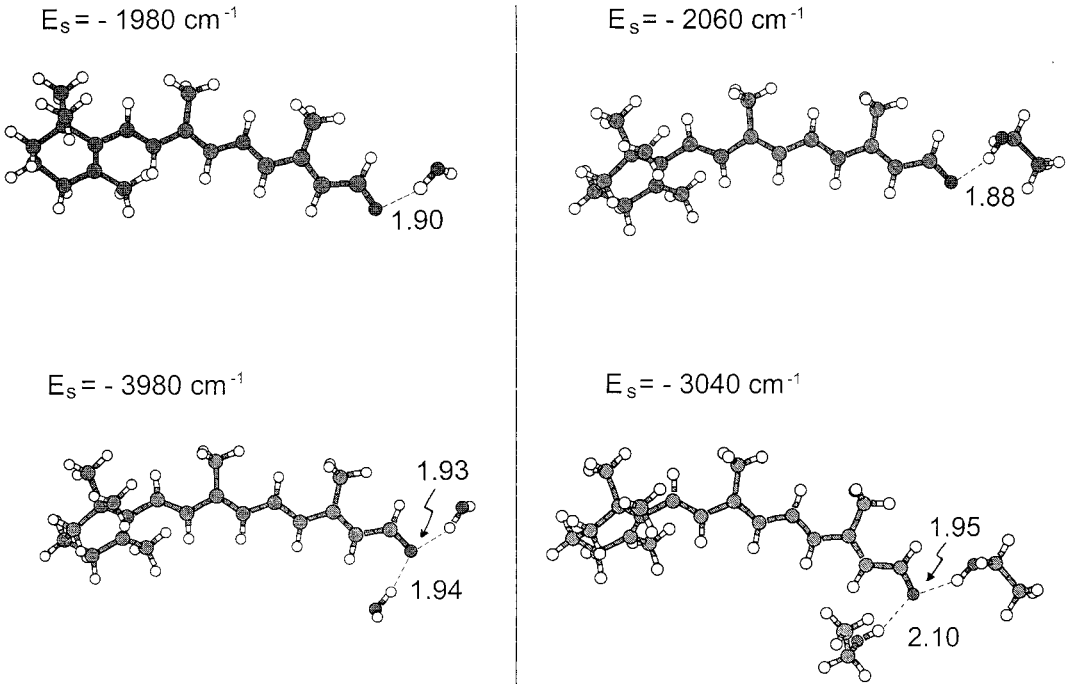

Figure 6. Calculated structure of the ATR 1:1 and 1:2 complexes with water (left) and ethanol (right) (DF calculation, B3-LYP functional, 6-31G* basis set) with relevant intermolecular distances (Å). For each complex the stabilization energy (E_s, cm^{-1}) is indicated on the upper left.

TABLE 2: Band Centers (ν_0) and Widths (Γ) of the Five Component Bands (A−E) Fitting the Observed ATR Fluorescence Spectra of Figures 2 and 3[a]

	A	B	C	D	E
ν_0 (cm^{-1})	22050	20640	19420	18220	16900
Γ (fwhm, cm^{-1})	5160	1660	2050	2270	1750

[a] A: S_3("B_u^+") → S_0 fluorescence of hydrogen-bonded species considered only for the 10^{-6} M solution; B and C: S_2("A_g^-") → S_0 fluorescence of the same species (1:1 and 1:2 complexes, respectively); D: dimer $|S_{3,D}^+>$ → $|G_D^+>$ transition; E: equivalent transition of the tetramer, as better explained in the text.

centered at 18220 cm^{-1} (≈549 nm), corresponds to an excitation band around 21700 cm^{-1} (≈460 nm), in close agreement with previous results.[27] The fourth component (band E of the Table 2), centered at 16900 cm^{-1} (≈591 nm), has no definite assignment on the basis of our solution data only. Since not only dimers of ATR and HATR but also tetramers (i.e., $(HATR)_4$ and $(ATR)_4$) are stable systems, according to our DF calculations B3-LYP/6-31G*, an assignment of the 16900 cm^{-1} band to emission from tetramers should be considered. The structure of $(ATR)_4$, shown in Figure 8 in a side view, consists of two weakly interacting pairs of dimers. Since the two pairs are not piled over each other, the central polyenic chains (average distance ≈4.95 Å) overlap only partially. On the contrary, the structure of each pair resembles closely that of the isolated dimer with chains ≈4.30 Å apart. All the energy data on the dimer and the tetramer are reported in Table 3.

It is interesting to note that under our experimental conditions no fluorescence can be observed from the free molecule even diluting considerably the solution. For instance, the fluorescence spectrum of a 10^{-6} M ATR solution at 77 K and with λ_{exc} = 355 nm is also shown in Figure 2. The spectrum has been fitted considering, in addition to previous bands, only a fifth Gaussian (band A of Table 2) centered at 22050 cm^{-1} with half-width 2580 cm^{-1}. Apparently, the free molecule S_3("B_u^+") fluorescence band (ν_{max} = 23250 cm^{-1}, half-width 1200 cm^{-1}, according to ref 24) is absent because of the extremely low quantum yield.[24] The 22050 cm^{-1} band may be tentatively related to the emission from S_3("B_u^+") of hydrogen-bonded species, known to coexist with free retinal S_3("B_u^+") species in protic solution.[26]

Let us now turn our attention to the crystal spectra of Figure 3. It may be seen, comparing with solution data, that while the low-energy (i.e., ≤19000 cm^{-1}) portion of the fluorescence emission is still observed, upper emission is missing. This indirectly supports the assignment of this spectral region (≥19000 cm^{-1}) to water complexes, considering the extensive drying operations carried out during this work on the polycrystalline sample. More quantitatively, only three Gaussian bands, centered as previously at 19420, 18220, and 16900 cm^{-1} and with the same widths, are necessary to fit the emission profiles

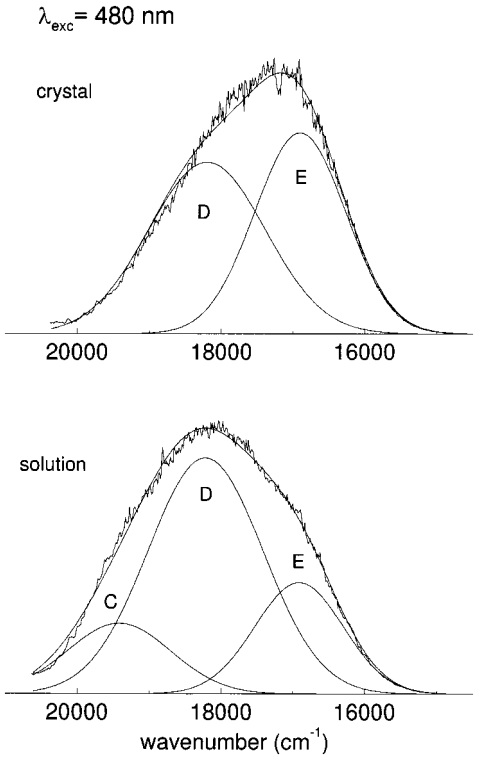

Figure 7. Spectral decomposition of the crystal (top) and solution (bottom; $c = 10^{-2}$ M) fluorescence spectra ($\lambda_{exc} = 480$ nm, 77 K) in terms of Gaussian bands. Capital letters refer to component bands as defined in Table 3.

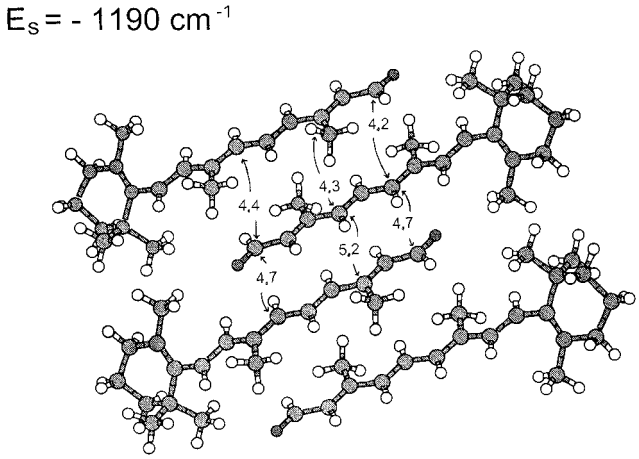

Figure 8. Calculated structure (side view) of $(ATR)_4$ (DF calculation, B3-LYP functional, 6-31G* basis set) with relevant intermolecular distances (Å). The average intrapair and interpair distances are 4.30 and 4.95 Å, respectively. The stabilization energy (E_s, cm^{-1}) is indicated on the upper left.

(see Figure 7, top panel, for a typical result). The 19420 cm^{-1} band, denoted as C in Table 2 and related to the 1:2 complexes with water, contributes ≤10% to the total emission intensity for $\lambda_{exc} = 420$, 440, and 460 nm and essentially nothing for the other two excitation wavelengths.

It may be also seen from Figure 3 that the largest fluorescence intensity corresponds to the 20800 cm^{-1} (≈480 nm) excitation. Excitation spectra have been measured on polycrystalline ATR at 77 K with the fluorescence window set at 16900 cm^{-1} (≈591 nm). The normalized signals were obtained from several measurements of incident and fluorescence intensities every 5 Å in the range 18000−23000 cm^{-1} (≈550−435 nm) and then averaging their ratio. The result, reported in Figure 9, shows

TABLE 3: Stabilization Energy with Respect to the Component Monomers of $(ATR)_n$ and $(HATR)_n$ ($n = 2, 4$) in Their Optimized Geometry (B3-LYP/DF calculation, 6-31G* basis set) Including the BSSE Correction

	E_s (cm^{-1})
$(ATR)_2$	−630
$(HATR)_2$	−605
$(ATR)_4$	−1190
$(HATR)_4$	−1250

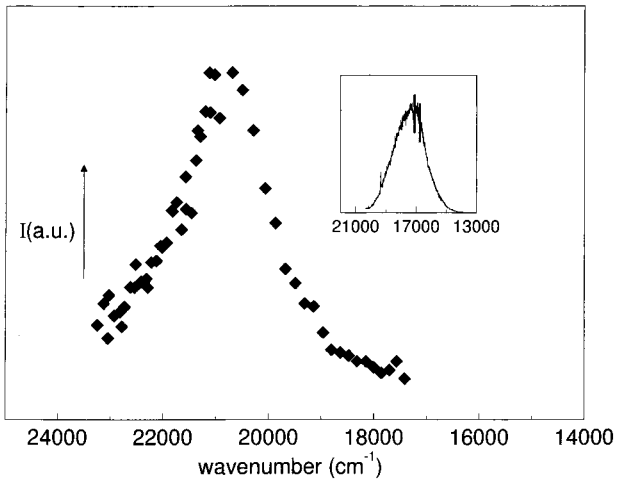

Figure 9. Normalized fluorescence excitation spectrum of polycrystalline ATR at 77 K. The energy of the excitation pulse was kept approximately constant, 10^{-2} mJ on the sample, in all the wavenumber ranges of interest. Inset: fluorescence spectrum ($\lambda_{exc} = 480$ nm, 77 K) with detection window set around 17000 cm^{-1} (≈590 nm).

that the broad excitation band with maximum around 20800 cm^{-1} is the absorption counterpart of the 16900 cm^{-1} emission band.

IV. Discussion

In this section the assignment of the two lowest energy emission bands (bands D and E of Table 2) is specifically discussed. In this context it is useful to recall that dimer states originate because of the intermolecular interaction between monomers.[43−45] The dipolar interaction between S_3("B_u^+") states of two ATR molecules, A and B, will be considered here. This is given[27] by the expression $V_{AB} = -(\mu^2_{S_0\rightarrow B_u^+}/R^3)(3\sin^2\theta - 2)$, where $\mu_{S_0\rightarrow B_u^+}$ is the transition $S_0 \rightarrow S_3$("B_u^+") point dipole with direction C_7-O,[15] R the distance between dipoles, and θ is the angle between the dipole direction and the line connecting the dipole baricenters. The energy term is positive and of the order $2\mu^2_{S_0\rightarrow B_u^+}/R^3$ for the tail-to-tail (i.e., →←) structure ($\theta = 0°$) and becomes negative as one polyenic chain slides above the other, up to $-\mu^2_{S_0\rightarrow B_u^+}/R^3$ for the ⇄ structure ($\theta = 90°$). Assuming that the latter is the effective arrangement between the transition dipoles of ATR in the dimer, the interaction energy, calculated from the molecular f value (1.18,[14] then $\mu^2_{S_0\rightarrow B_u^+} \approx 9.6$ D) is ≈−6000 cm^{-1} with $R = 4.25$ Å. The ground and excited dimer states may be expressed in a first approximation as "plus" (g) and "minus" (u) linear combinations of monomer states: i.e., $|G_D^{\pm}\rangle = (1/\sqrt{2})(S_{0,A} \pm S_{0,B})$ and $|S_{3,D}^{\pm}\rangle = (1/\sqrt{2})[S_{3,A}(B_u^+) \pm S_{3,B}(B_{u,B}^+)]$. Since the interaction energy between S_3("B_u^+") states is negative, the lowest excited dimer state is of g symmetry. Band D is assigned to the dipole forbidden $|S_{3,D}^+\rangle \rightarrow |G_D^+\rangle$ transition, made allowed only through vibronic coupling of $|S_{3,D}^+\rangle$ with $|S_{3,D}\rangle$. If the equilibrium geometries of the $|G_D^+\rangle$ and $|S_{3,D}^+\rangle$ states are not much different, the energy gap ΔE_{d-m} between the dimer $|S_{3,D}^+\rangle \rightarrow |G_D^+\rangle$ and

the monomer S_3("B_u^+") → S_0 transitions is calculated to a first approximation to be -5400 cm^{-1}, considering the ground-state stabilization (≈ -600 cm^{-1}; see Table 3). Experimentally, ΔE_{d-m} may be estimated from the fluorescence spectrum of the molecule[24] in combination with our results on the 10^{-2} M solution. At room temperature the S_3("B_u^+") → S_0 fluorescence maximum of the free molecule is found[24] at $\approx$23250 cm^{-1}. Neglecting for the sake of simplicity the temperature dependence of the band centers and since the dimer fluorescence maximum is at $\approx$18220 cm^{-1}, the calculated ΔE_{d-m} (-5400 cm^{-1}) closely approaches the experimental value (-5030 cm^{-1}).

When four interacting transition dipoles are considered the tetramer gap with respect to the monomer, ΔE_{t-m}, may be roughly estimated on the basis of the structural data on $(ATR)_4$ of Figure 8 and taking into account only the dipolar interactions between nearest neighbors. To this purpose, in addition to $V_{1,2} = V_{3,4} \approx -5800$ cm^{-1} (each intrapair distance, $R_{1,2}$ and $R_{3,4}$, of the tetramer on average being 4.30 Å), it is necessary to calculate $V_{2,3}$, the interaction between inner transition dipoles. As the central molecules do not fully overlap in the tetramer structure, $V_{2,3}$ is expected to be smaller than $V_{1,2}$. It is easy to show that with $V_{1,2} = -5800$ cm^{-1} and $V_{2,3} = -2900$ cm^{-1}, ΔE_{t-m} is ≈ -6240 cm^{-1}, after diagonalization of the 4×4 interaction matrix (eigenvalues: ± 7430, ± 4530 cm^{-1}), considering the lowest eigenvalue, -7430 cm^{-1}, and the tetramer stabilization energy in the ground state ($E_s \approx -1190$ cm^{-1}; see Table 3). In other words, the tetramer emission maximum is expected to occur at 23250 cm^{-1} − 6240 cm^{-1} = 17010 cm^{-1}. This gives confidence to our proposed assignment of the E band (see Table 2) as the transition from the lowest component of the "B_u^+" quartet to the corresponding ground state. Because of the approximations used in the model, it is obvious that the result should not be taken too literally but rather as a positive indication that the transition energy in $(ATR)_4$ is appreciably lower than in $(ATR)_2$.

The spectral analysis of the last section has shown that crystal and solution fluorescence (in the low-energy portion) are fitted by the same Gaussian bands centered at 18220 and 16900 cm^{-1}. The similarity of behavior strongly supports the view that the systems responsible for the radiative relaxation are the same. On this basis the crystal bands are assigned to fluorescence from dimers and more associated clusters (likely, tetramers), respectively. This implies that these species may be identified in the crystal structure of ATR. It is, in fact, well-known, at least in the case of excimer fluorescence from crystals, that a basic condition for the effect is the ability of the structure to accommodate sandwich-like pairs of molecules.[46] The crystal structure of ATR is monoclinic, space group C_{2h}^5 ($P_{2_{1/n}}$), with four molecules per unit cell in general position.[47] Taking the crystal coordinates of the molecule in the (0,0,0) cell[47] and of a second resulting from inversion symmetry and translation in the cell (−1,0,−2) and repeating the procedure along the monoclinic *b* axis, the structure shown in Figure 10 is obtained. It may be seen that the molecules in the cells $(0,-n,0)$ and $(-1,-n,-2)$ are stacked in columns with an easily distinguished dimer geometry with averaged intrapair distance $\approx$4.0 Å. In addition, the dimers are located with respect to each other according to an arrangement quite similar to that found in the tetramer case with interpair distance $\approx$4.6 Å.

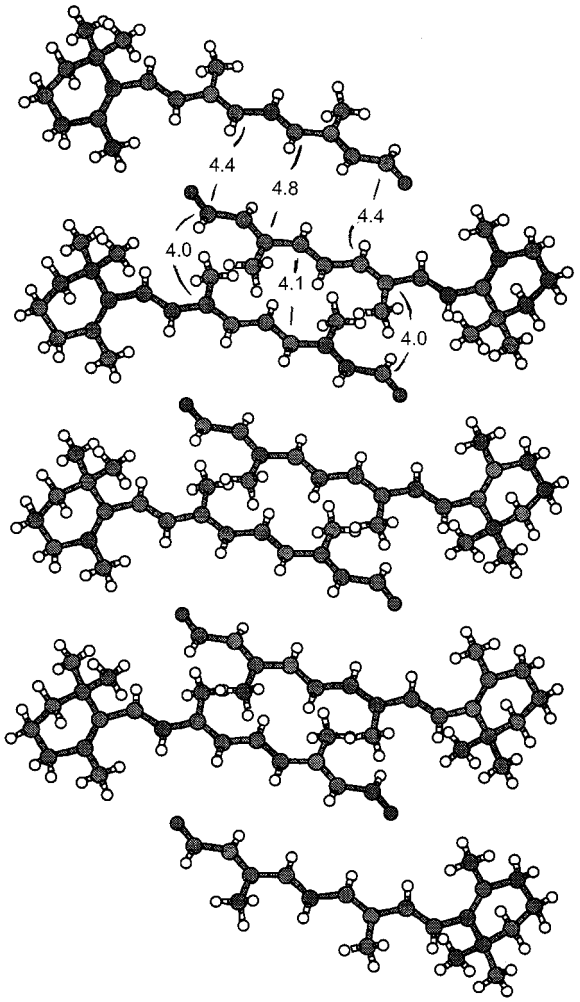

Figure 10. Crystal structure of ATR along the *b* monoclinic axis with relevant intermolecular distaces (Å): the molecule in the cell $(0,-n,0)$ and the molecule obtained by inversion of center and translation in the cell $(-1,-n,-2)$ are considered. The average intrapair and interpair distances are 4.0 and 4.6 Å, respectively.

V. Conclusions

In this paper radiative relaxation processes of ATR as a polycrystalline sample and in concentrated solutions have been investigated at 77 K as a function of the exciting wavelength below the threshold of the molecular absorption. The crystal fluorescence has been observed for the first time at low temperature. Emissions from hydrogen-bonded complexes and retinal clusters have been observed in solution, while only from the latter species in the crystal case. High-quality B3-LYP/6-31G* DF calculations show that $(ATR)_n$ and $(HATR)_n$ ($n = 2$, 4) are ground-state stable species. These species have excited states at energy lower than $S_1(n\pi^*)$ of the monomer. New relaxation channels are available to the crystal leading ultimately to these states rather than to $S_1(n\pi^*)$ and therefore to the efficient fluorescence quenching from the lowest singlet states of the monomer.

Acknowledgment. This work was supported by the Italian Consiglio Nazionale delle Ricerche (CNR) and by the Ministero dell'Università e della Ricerca Scientifica e Tecnologica (MURST). The authors thank CINECA (Bologna, Italy) for providing computer time.

References and Notes

(1) Birge, R. R. *Biochim. Biophys. Acta* **1990**, *1016*, 293−327.

(2) Wang, Q.; Schoenlein, R. W.; Peteanu, L. A.; Mathies, R. A.; Shank, C. V. *Science* **1991**, *264*, 412−415.

(3) Logunov, S. L.; Song, L.; El-Sayed, M. A. *J. Phys. Chem.* **1996**, *100*, 18586−18591.
(4) Garavelli, M.; Vreve, T.; Celani, P.; Bernardi, F.; Robb, M. A.; Olivucci, M. *J. Am. Chem. Soc.* **1998**, *120*, 1285−1288.
(5) Hahn, S.; Stock, G. *J. Phys. Chem. B* **2000**, *104*, 1146−1149.
(6) Takemura, T.; Das, P. K.; Hug, G.; Becker, R. S. *J. Am. Chem. Soc.* **1978**, *100*, 2626−2630.
(7) Song, P. S.; Chae, Q.; Fujita, M.; Baba, H. *J. Am. Chem. Soc.* **1976**, *98*, 819−824.
(8) Becker, R. S. *Photochem. Photobiol.* **1988**, *48*, 369−399.
(9) Becker, R. S.; G., H.; Das, P. K.; Schaffer, A. M.; Takemura, T.; Yamamoto, N.; Waddell, W. H. *J. Phys. Chem.* **1976**, *80*, 2265−2273.
(10) Bensasson, R.; Land, E. J.; Truscott, T. G. *Photochem. Photobiol.* **1975**, *21*, 419−421.
(11) Rosenfeld, T.; Alchalel, A.; Ottolenghi, M. *J. Phys. Chem.* **1974**, *78*, 336−341.
(12) Veyret, B.; Davis, S. G. nad Yoshida, M.; Weiss, K. *J. Am. Chem. Soc.* **1978**, *100*, 3283−3290.
(13) Yamaguchi, S.; Hamaguchi, H. *J. Chem. Phys.* **1998**, *109*, 1397−1409.
(14) Birge, R. R.; Bennett, J. A.; Hubbard, L. M.; Pierce, H. F.; Kliger, D. S.; Leroi, G. E. *J. Am. Chem. Soc.* **1982**, *104*, 2519−2525.
(15) Drikos, G.; Morys, P.; Ruppel, H. *Photochem. Photobiol.* **1984**, *40*, 133−135.
(16) Drikos, G.; Ruppel, H. *Photochem. Photobiol.* **1984**, *40*, 93−104.
(17) Birge, R. R. *Acc. Chem. Res.* **1986**, *19*, 138−146.
(18) Birge, R. R.; Pierce, H. F. *J. Chem. Phys.* **1979**, *70*, 165−178.
(19) Tallent, J. R.; Birge, J. R.; Zhang, C. F.; Wenderholm, E.; Birge, R. R. *Photochem. Photobiol.* **1992**, *56*, 935−952.
(20) Merchan, M.; Gonzalez-Luque, R. *J. Chem. Phys.* **1997**, *106*, 1112−1122.
(21) Weimann, L. J.; Maggiora, G. M.; Blatz, P. E. *Int. J. Quant. Chem.* **1975**, *2*, 9−24.
(22) Takemura, T.; Das, P. K.; Hug, G.; Becker, R. S. *J. Am. Chem. Soc.* **1976**, *90*, 7099−7101.
(23) Das, P. K.; Becker, R. S. *J. Phys. Chem.* **1978**, *82*, 2093−2105.
(24) Takeuchi, S.; Tahara, T. *J. Phys. Chem.* **1997**, *101*, 3052−3061.
(25) Tahara, T.; Hamaguchi, H. *Chem. Phys. Lett.* **1995**, *234*, 275−280.
(26) Yamaguchi, S.; Hamaguchi, H. *J. Phys. Chem. A* **2000**, *104*, 4272−4279.
(27) Takemura, T.; Hug, G.; Das, P. K.; Becker, R. S. *J. Am. Chem. Soc.* **1978**, *100*, 2631−2634.
(28) Gervasio, F. L.; Cardini, G.; Salvi, P. R.; Schettino, V. *J. Phys. Chem.* **1998**, *102*, 2131−2136.
(29) Gellini, C.; Salvi, P. R.; Hafner, K. *J. Phys. Chem.* **1993**, *97*, 8152−8157.
(30) Catani, L.; Gellini, C.; Salvi, P. R. *J. Phys. Chem.* **1998**, *102*, 1945−1953.
(31) Birge, R. R.; Bocian, D. F.; Hubbard, L. M. *J. Am. Chem. Soc.* **1982**, *104*, 1196−1207.
(32) Das, P. K.; Becker, R. S. *J. Phys. Chem.* **1978**, *82*, 2081−2093.
(33) Drikos, G.; Ruppel, H.; Sperling, W.; Morys, P. *Photochem. Photobiol.* **1984**, *40*, 85−91.
(34) Becker, R. S.; Inuzuka, K.; Balke, D. E. *J. Am. Chem. Soc.* **1971**, *93*, 38−42.
(35) Christensen, R. L.; Kohler, B. E. *Photochem. Photobiol.* **1973**, *18*, 293−301.
(36) Christensen, R. L.; Kohler, B. E. *Photochem. Photobiol.* **1974**, *19*, 401−410.
(37) Becke, A. D. *Phys. Rev. A* **1988**, *33*, 3098−3100.
(38) Lee, C.; Yang, W.; Parr, R. G. *Phys. Rev. B* **1988**, *37*, 785−789.
(39) Boys, S. F.; Bernardi, F. *Mol. Phys.* **1970**, *19*, 553−566.
(40) van Duijneveldt, F. B.; van Duijneveldt-van de Rijdt, J. G. C. M.; van Lenthe, J. H. *Chem. Rev.* **1994**, *94*, 1873−1885.
(41) Personov, R. I. In *Spectroscopy and excitation dynamics of condensed molecular crystals*; Agranovich, V. M., Hochstrasser, R. M. Eds.; North-Holland: Amsterdam, 1983; p 555.
(42) Warshel, A.; Karplus, M. *J. Am. Chem. Soc.* **1974**, *96*, 5677−5689.
(43) Azumi, T.; McGlynn, S. P. *J. Chem. Phys.* **1964**, *41*, 3131−3138.
(44) Azumi, T.; Armstrong, A. T.; McGlynn, S. P. *J. Chem. Phys.* **1964**, *41*, 3839−3852.
(45) Klessinger, M.; Michl, J. *Excited States and Photochemistry of Organic Molecules*; VCH Publishers: New York, 1995.
(46) Stevens, B. *Spectrochim. Acta* **1962**, *18*, 439−448.
(47) Hamanaka, T.; Mitsui, T.; Ashida, T.; Kakudo, M. *Acta Crystallogr. B* **1972**, *28*, 214−222.